ACS Sustainable Chemistry & Engineering

Research Article

pubs.acs.org/journal/ascecg

Facile Fabrication of Pt Nanoparticles on 1-Pyrenamine Functionalized Graphene Nanosheets for Methanol Electrooxidation

Lihua Li,[†] Jianan Zhang,[†] Yuqing Liu,[†] Weimin Zhang,[‡] Hongxia Yang,[†] Jun Chen,[§] and Qun Xu*,[†]

[†]College of Materials Science and Engineering, Zhengzhou University, Zhengzhou 450052, China

[‡]Centre for Sustainable Energy Development, School of Chemical and Biomolecular Engineering, Faculty of Information and Engineering, University of Sydney, New South Wales 2006, Australia

[§]ARC Centre of Excellence for Electromaterials Science, Intelligent Polymer Research Institute, University of Wollongong, New South Wales 2522, Australia

ABSTRACT: In this paper, noncovalent functionalized graphene nanosheets are prepared through solvent-exfoliation expanded graphite with the aid of supercritical (SC) CO_2 and 1-pyrenamine (PA). Then, it is used as supporting materials for platinum to investigate the potential application of the obtained nanocomposite in direct methanol fuel cells (DMFCs). Transmission electron microscope (TEM) images reveal that Pt nanoparticles are evenly dispersed on the PA-modified graphite nanosheets (PA-GNS) with an average size of 3.0 nm. The high quality of PA-GNS is also confirmed through Raman spectra analysis. PA-GNS/Pt nanocomposites exhibit better electrocatalytic activity (1.4 times) and stability (3.5 times) toward methanol oxidation than commercial catalyst JM-C/Pt. The results suggest that noncovalent functionalization of GNS by PA can be a method used to create highly efficient and stable catalyst supports for methanol electrooxidation in DMFCs.

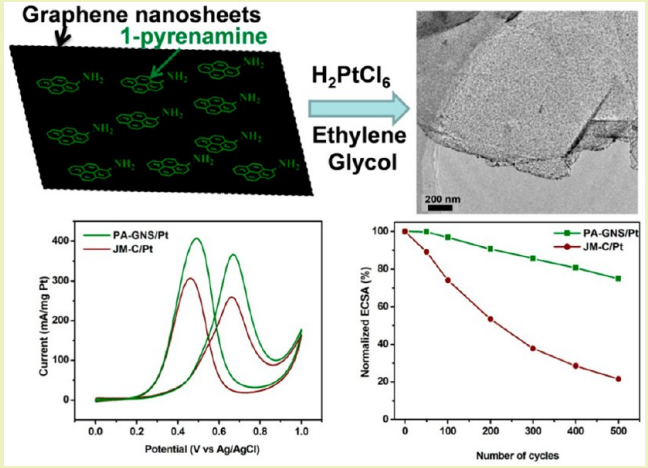

KEYWORDS: *Graphene nanosheets, Noncovalent functionalization, Pt nanoparticles, Methanol electrooxidation*

INTRODUCTION

Due to the depletion of fossil fuels and the increasing concerns of environmental protection, new power sources are in great demand.[1−4] Direct methanol fuel cells (DMFCs) are considered as an excellent candidate owing to their ease of handing, high-energy conversion efficiency, low pollutant emission, and low operating temperatures.[5,6] The noble metal platinum (Pt) is one of the best catalysts for DMFCs.[7−13] However, the high cost and low electrocatalytic activity and stability of common Pt catalyst inhibit the broad applications of DMFCs.[10,14] In order to improve the performance of Pt catalyst in the DMFCs, an efficient method is to incorporate Pt nanoparticles with carbonaceous materials, such as carbon black (CB),[15,16] carbon nanotubes (CNTs),[17−20] carbon nanofibers (CNFs)[21,22] and graphene.[23−25]

Graphene, a kind of two-dimensional sheet which is composed of sp^2-bonded carbon atoms, exhibits outstanding physicochemical properties, such as high specific surface area and excellent electronic conductivity and resistance to corrosion, making it an ideal catalyst support for fuel cell application.[26−29] But pristine graphene is relatively inert, and the metal particles are typically weakly adsorbed on graphene and easy to diffuse along the surface,[30] which lead to catalyst sintering and loss of catalytic activity.[31] Among the reported methods, graphene oxide (GO) flakes or reduced graphene oxide (RGO) flakes are widely used as the support materials for catalyst.[24,25,32,33] The oxygen groups in the GO or RGO not only increase the hydrophilicity of the graphene but also provide the active site for anchoring metal nanoparticles on the surface of graphene.[34,35] However, the oxidization treatments damage the desirable properties of the graphene and make it easy to corrode under harsh electrochemical conditions.[36] So noncovalent functionalization of graphitized carbons with organic bifunctional molecules through $\pi-\pi$ interactions is an effective strategy.[37] Li et al.[38] and Oh et al.[39] have efficiently loaded Pt nanoparticles on CNTs and CNFs using 1-pyrenamine (PA) as an interlinker.

Our previous study indicated that graphene could be exfoliated and functionalized from graphite with the aid of the syngenstic effect of pyrene-derivatives and supercritical carbon dioxide (SC CO_2).[40,41] High quality and noncovalent functionalized graphene were successfully prepared, and they are expected to have potential use as catalyst supports. In this paper, we report a facile method to prepare Pt nanoparticles

Received: January 6, 2013
Revised: February 27, 2013
Published: March 4, 2013

   dx.doi.org/10.1021/sc4000016 | *ACS Sustainable Chem. Eng.* 2013, 1, 527−533

supported on noncovalent functionalized graphene nanosheets (GNS) that were prepared by exfoliation of expanded graphite in DMF with the assistance of PA and SC CO_2. Then, we study its potential application for DMFCs. Moreover, the effects of PA on the dispersion of Pt nanoparticles and electrocatalyst performance are also investigated. This suggests that PA noncovalent-functionalized graphene nanosheets are desirable supporting materials for noble metal catalysts in DMFCs.

EXPERIMENTAL SECTION

Materials. Expandable graphite with average particles 150 μm was purchased from Qingdao Jinrilai Electronic Material Company (Qingdao, China). 1-Pyrenamine (PA) (>98%) was purchased from Tokyo chemical industry Co., Ltd. (Japan). H_2PtCl_6 was purchased from Aldrich. Nafion 117 (5 wt %) was purchased from Aldrich. CO_2 (99.95%) was supplied by Zhengzhou Shuangyang Gas Co. (China). All other reagents employed were supplied by Guangdong guanghua Sci-Tech Co., Ltd. (China) and used as received. Deionized water was used to prepare aqueous solutions.

Preparation of Noncovalent Functionalized GNS. GNS were produced by exfoliating the expanded graphite with the assistance of PA and SC CO_2. First, expandable graphite was rapidly expanded in a commercial microwave oven (Galanz, 700 W, 30 s) under atmosphere. A 20 mg portion of expanded graphite and 6 mg PA were dispersed into 10 mL DMF through sonication for 2 h. Then, the mixture was transferred into the high-pressure stainless steel reactor and CO_2 was charged into the reactor to presetting condition (40 °C, 16 MPa). The resulting mixture was sonicated for 3 h. The sample was then centrifuged and washed with ethanol three times at 9000 rpm for 15 min to remove the free PA. Finally, the product was dried at 60 °C overnight and denoted as PA-GNS. GNS without PA was also prepared using the same methods.

Synthesis of PA-GNS/Pt and GNS/Pt Composites. In a typical experiment, 10 mg PA-GNS (or GNS) was dispersed into 20 mL ethylene glycol by sonication for 30 min. H_2PtCl_6 aqueous solution (0.254 mL, 50.47 mM) was thereafter added and stirred with a magnetic stir bar for 1 h. The solution was then refluxed at 130 °C for 4 h. And the solution was settled overnight, centrifuged, and washed with ethanol three times. Finally, the solid catalyst was dried in an oven at 60 °C overnight and denoted as PA-GNS/Pt (or GNS/Pt). The theoretical Pt loading is 20 wt %. Commercial Pt/Vulcan XC-72R (Johnson Matthey, Pt loading: 20 wt %) was used as a reference for comparison and denoted as JM-C/Pt.

Characterization. Transmission electron microscopy (TEM) was performed with a JEM-2100 operating at 200 kV. Scanning electron microscopy (SEM) was carried out with a JEOL JSM-7500F field emission scanning electron microscope. Energy dispersive X-ray spectroscopy (EDS) was recorded with an Oxford INCA 250 energy-dispersive spectrometer equipped on the microscope. Power X-ray diffraction (XRD) patterns were performed using a Rigaku/Max-3B with Cu Kα radiation (λ = 0.15418 nm). UV−vis absorption spectra were measured at room temperature with a Shimadzu UV-240/PC spectrophotometer. Raman spectra were carried out at 532 nm using a Renishaw invia Raman Microscope at room temperature. Thermogravimetry (TG) was conducted on a STA449C thermogravimetric analyzer from room temperature to 800 °C at 10 °C min^{-1} under air flow.

Electrochemical Activity Characterization. All the electrochemical measurements were finished using CHI 660D electrochemical workstation. A conventional three electrode cell was employed with a Pt wire as the counter electrode, a statured Ag/AgCl electrode as the reference electrode, and a glassy carbon (GC) electrode (diameter = 5 mm) with coated catalysts serving as the working electrode. About 7.44 μg Pt of the catalyst was loaded on the glass carbon disk; the loading of Pt is about 38.0 μg cm^{-2}.

The electrochemical active surface area (ECSA) values and electrocatalytic activity for the methanol oxidation of the catalyst were measured in N_2-statured 0.5 M H_2SO_4 solution and 0.5 M H_2SO_4 containing 1 M methanol solution by cyclic voltammetry (scan rate: 25 mV s^{-1}) at room temperature. Accelerated durability test (ADT) was carried out by CV measurements in the range of 0.5−1.0 V (vs Ag/AgCl) at 50 mV s^{-1} in N_2-statured 0.5 M H_2SO_4 solution.

RESULTS AND DISCUSSION

The processes of synthesis of graphene nanosheets/Pt composite and 1-pyrenamine (PA) modified graphene nanosheets/Pt composite are schematically illustrated in Scheme 1.

Scheme 1. Schematic Illustration of the Synthesis of Graphene Nanosheets/Pt Composite and 1-Pyrenamine (PA) Modified Graphene Nanosheets/Pt Composite, Respectively

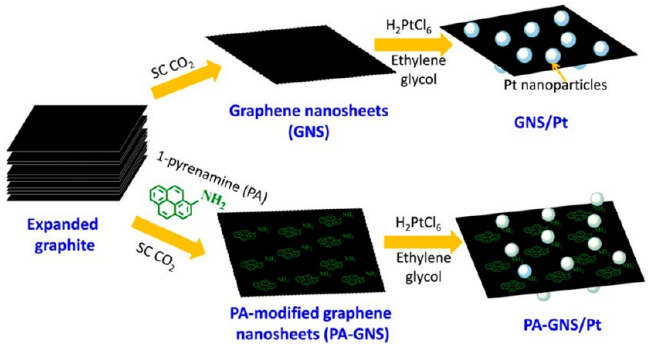

As for the PA-GNS/Pt, expanded graphene was first exfoliated into few-layer graphene nanosheets with the synergestic effect of supercritical carbon dioxide (SC CO_2) and PA. The low-viscosity and high-diffusivity of SC CO_2 facilitate the penetration and intercalation of PA and solvent between the inner layer of graphite.[40,41] The pyrenyl group of PA strongly adsorbs onto the surface of GNS via $\pi-\pi$ interaction,[38] and the amine ($-NH_2$) group is introduced at the same time. Then H_2PtCl_6 is mixed with the PA-GNS and reduced by ethylene glycol. The amine groups of PA-GNS can act as active sites for the nucleation and growth of Pt nanoparticles and enhance the interaction between graphene nanosheets and Pt nanoparticles. The pristine structure of the graphene nanosheet is preserved perfectly through this noncovalent functionalization method.

Figure 1 shows the SEM images of the expanded graphite flakes. The expanded graphite shows typical worm-like

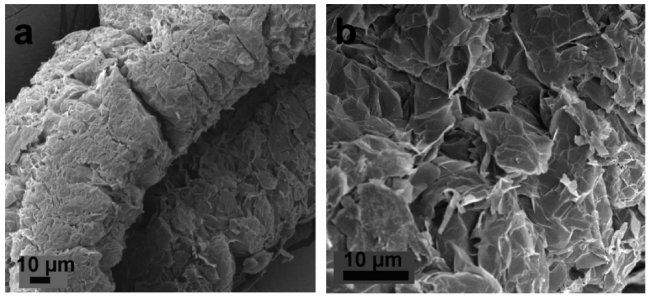

Figure 1. (a) Low- and (b) high-magnification SEM images of expanded graphite.

morphologies and loose structure (Figure 1a). From the higher-magnification image (Figure 1b), we can see clearly that graphite flakes with a lateral size of approximately 10−80 μm randomly stack together. The loose structure is desirable for the following solvent exfoliation.

dx.doi.org/10.1021/sc4000016 | ACS Sustainable Chem. Eng. 2013, 1, 527−533

After exfoliation by SC CO_2 and sonication, the dispersion of PA-GNS was washed with ethanol by centrifugation to remove the free PA molecule. Then the dispersion of GNS, PA-GNS, and pure PA was characterized via UV−vis absorption spectra. As shown in Figure 2, free PA molecules exhibited absorption

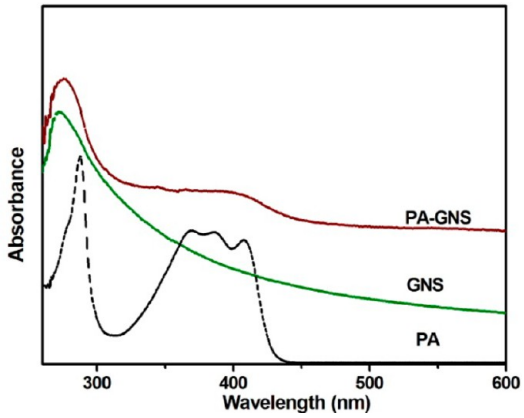

Figure 2. UV−vis absorption spectra of PA, GNS, and PA-GNS.

peaks at λ = 288, 367, 386, and 413 nm and the GNS dispersion showed one absorption peak at λ = 270 nm. PA-GNS showed a strong absorption peak located at 275 nm corresponding to GNS with a redshift (λ = 5 nm) and a broad absorption band around 400 nm corresponding to the PA molecule. PA is an aromatic compound with large planar aromatic structures of pyrene that can strongly anchor themselves onto the surface of graphene nanosheets through $\pi-\pi$ interaction. So, the spectra indicated that PA has successfully attached on the surface of GNS.[37,38,41]

Zoval et al.[42] have reported that Pt particles nucleate preferentially at the step edges and point defects of graphite basal plane. Most of the previous reports for GO/Pt nanocomposites reflected that the abundant functional groups such as carbonyls, hydroxyls, and epoxides on GO make it a good support for Pt depositing.[24,25] These functional groups can act as active sites for enhancing the binding of metal particles to graphite and increase the stability of metal particles toward sintering. We expect that the amine groups attached on the PA-GNS will have these functions.

The morphology of GNS/Pt and PA-GNS/Pt nanocomposites were explored by SEM. As shown in Figure 3a and b, GNS consisted of flakes with a lateral size ranging from 0.5 to 20 μm. These phenomena indicated that expanded graphite was successfully exfoliated into graphene nanosheets with the assistance of SC CO_2. From the high-magnification SEM images of GNS/Pt and PA-GNS/Pt (Figure 3c and d), we

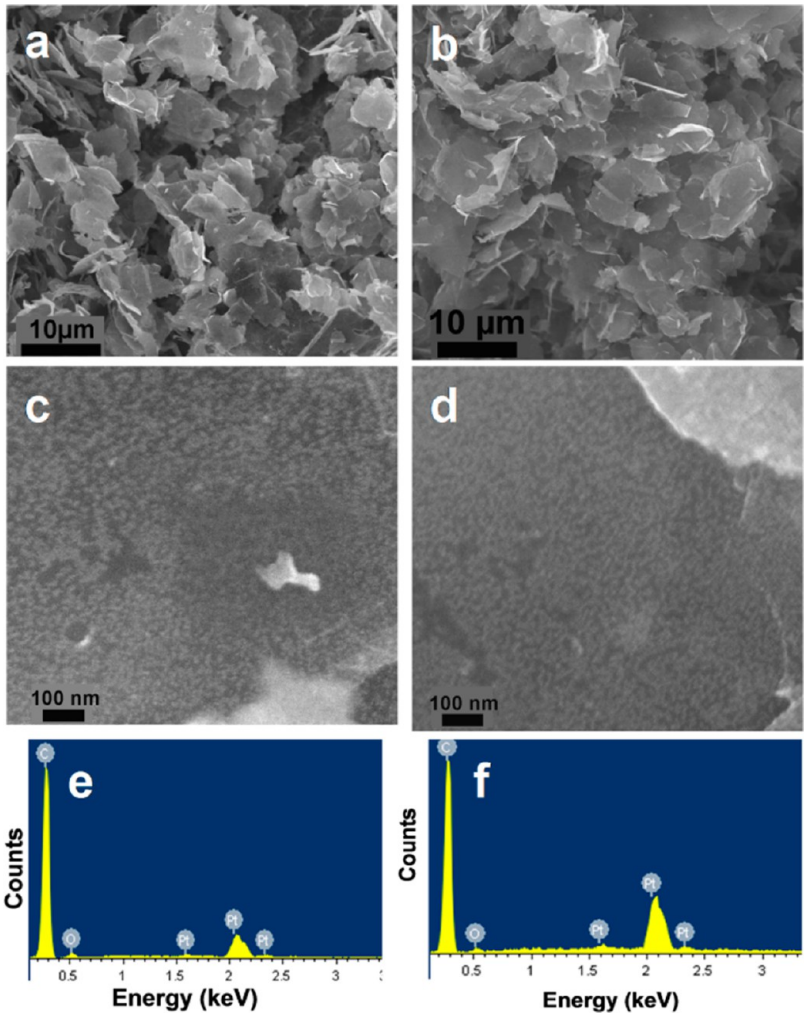

Figure 3. Low- and high-magnification SEM images and EDS spectra of GNS/Pt (a, c, and e) and PA-GNS/Pt (b, d, and f) nanocomposites.

dx.doi.org/10.1021/sc4000016 | ACS Sustainable Chem. Eng. 2013, 1, 527−533

can find that Pt nanoparticles have successfully deposited on the surface of GNS and PA-GNS. In the case of PA-GNS/Pt, the Pt particles are more dense and uniform than GNS/Pt, suggesting that the PA molecular can effectively attract and stabilize Pt particles on GNS, leading to a high dispersion of Pt particles. The EDS spectra of GNS/Pt and PA-GNS/Pt (Figure 3e and f) reveal the presence of C, O, and Pt on both samples, providing further evidence that Pt nanoparticles were formed on the surface of GNS. Apparently the enrichment of Pt in the latter sample is much higher. According to the TG analysis, the loading of Pt for PA-GNS/Pt is 18.6%, while the loading of Pt on GNS is 17.1%. The increased yield improved the utilization rate of noble metal Pt and reduced the cost of catalyst preparation.[39]

The above studies have shown that PA played a role in improving the loading of Pt on GNS. In the following study, we investigated the effect of PA on the size and distribution of Pt nanoparticles. The crystalline nature of the Pt nanoparticles was investigated by X-ray diffraction (XRD). As shown in Figure 4,

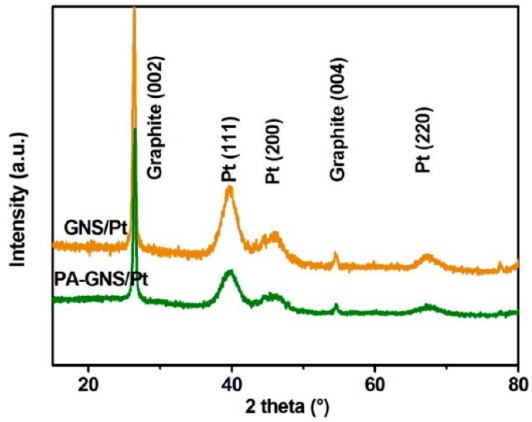

Figure 4. XRD patterns of GNS/Pt and PA-GNS/Pt.

both PA-GNS/Pt and GNS/Pt composite show distinct diffraction peaks at 39.5°, 45.9°, and 67.4° corresponding to the (111), (200), and (220) planes of fcc structure of Pt, respectively. Meanwhile, the diffraction peaks at 26.5° is attributed to the (002) reflection of GNS, indicating that the GNS is composed by multilayer graphene sheets.[32] It can be suggested that we have successfully prepared the GNS/Pt composite. It has been reported that the average size of Pt nanoparticles can be calculated according to Scherrer's formula.[43] From the full width half-maximum of the Pt (220) peak, the average particles sizes of Pt on GNS/Pt and PA-GNS/Pt were 3.6 and 2.7 nm, respectively.

The morphologies, size, and dispersion of Pt particles supported on the GNS and PA-GNS were further investigated by TEM. Figure 5 is the TEM images and corresponding histograms of Pt particle size distributions of the GNS/Pt and PA-GNS/Pt. The 100 randomly chosen particles were used to analyze the size distribution of Pt. As shown in Figure 5c, the Pt particles deposited on the GNS with diameters ranging from 2 to 6 nm. The average particles size of GNS/Pt is 4.0 nm. For PA-GNS/Pt (Figure 5d and e), the mean sizes of Pt particles is smaller (3.0 nm). This can be attributed to the large amount of amine ($-NH_2$) groups introduced by the PA molecules which can act as active sites for the nucleation of Pt nanoparticles and restrict the growth of the particle.[44] The inset of Figure 5d shows an fcc Pt(111) plane with a *d*-spacing value of 0.22 nm.[33] The size and dispersion of Pt nanoparticles on the supports are highly responsible for the electrocatalytic activity of methanol oxidation.[37]

Carbon black has been widely used as catalyst supporting materials. However, the biggest drawback of the carbon black is prone to electrochemical corrosion.[16,45] Graphitized carbon has been considered as a good substitute for its superior corrosion resistance.[18,37] The Raman spectrum was widely used to study the structure and defects of carbon materials. Herein, we identified the quality of GNS/Pt and PA-GNS/Pt by Raman spectroscopy. Commercial Pt/Vulcan XC-72R (JM-C/Pt) was also characterized for comparison. As shown in Figure 6, the band at about 1355 cm^{-1} corresponds to the defects induced D band and the band at 1587 cm^{-1} corresponds to the E_{2g} phonon of sp^2 atoms (G band). The greater the intensity of the D band, the more defects the carbon materials possess. Generally, the intensity ratio of D and G (I_D/I_G) can be used to evaluate the degree of graphitization of the carbon materials.[46] JM-C/Pt has the highest intensity of D band and a higher I_D/I_G (1.28), implying that there are a large number of defects in JM-C/Pt and the degree of graphitization is rather low. On the contrary, both GNS/Pt and PA-GNS/Pt have a very weak D band, and the I_D/I_G for GNS/Pt and PA-GNS/Pt is 0.17 and 0.18, respectively. This indicates that the defect densities of GNS/Pt and PA-GNS/Pt are very low and the high degree of graphitization is maintained. Therefore, we believe that the catalysts prepared by our methods will be more stable than JM-C/Pt under the same electrochemical conditions.

The electrocatalytic activity of PA-GNS/Pt as a potential electrocatalyst for the DMFCs was examined. The electrochemical active surface area (ECSA) is generally closely related to the electrocatalytic activity of the catalysts.[19] Figure 7a illustrated the CV curves of different samples in N_2-satureated 0.5 M H_2SO_4 solution with a potential range from −0.2 to 1.0 V vs Ag/AgCl at a potential scan rate of 25 mV s^{-1}. The values of ECSA were calculated from the hydrogen adsorption charge in the negative-going potential scan on CVs after double-layer correction.[19,47] The estimated ECSA values are the following: 82.9 (PA-GNS/Pt), 64.0 (JM-C/Pt) and 42.7 m^2 g^{-1} (GNS/Pt). PA-GNS/Pt has the highest value of ECSA, which is consistent with improved dispersion, small size, and narrow size distribution of the Pt on the PA-GNS support.[32] It is suggested that the PA-GNS/Pt would be favorable toward electrochemical reaction.

The electrocatalytic properties of GNS/Pt and PA-GNS/Pt toward the methanol oxide reaction (MOR) were measured and compared with those of JM-C/Pt. Figure 7b presents the CV profiles for GNS/Pt, PA-GNS/Pt, and JM-C/Pt for the MOR in a solution of 0.5 M H_2SO_4 + 1 M CH_3OH at room temperature. All catalysts show a similar CV curve, a forward peak around 0.7 V versus Ag/AgCl originates from the oxidation of methanol, and a backward peak around 0.5 V versus Ag/AgCl originates from the oxidation of intermediate carbonaceous species.[48] The mass-specific peak current density in the forward sweep for the PA-GNS/Pt is 365.6 mA mg^{-1}, which is higher than that of JM-C/Pt (105.0 mA mg^{-1}) and 4.3 times than that of the GNS/Pt of 85.6 mA mg^{-1}. The enhanced catalytic activity for MOR of PA-GNS/Pt may be attributed to the following: first, the utility of PA improves the distribution of Pt nanoparticles on the GNS with smaller sizes, thus introducing more active sites of Pt.[37] Second, the intrinsic properties of GNS are preserved perfectly with this non-destructive PA functionalization method, such as high

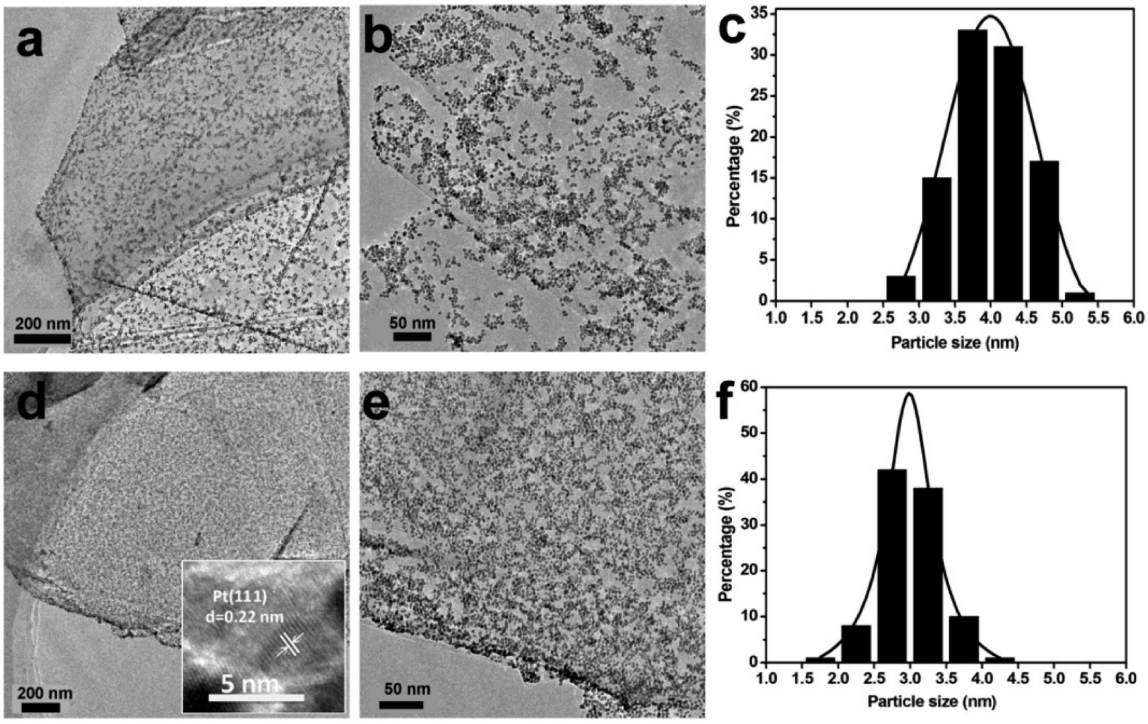

Figure 5. Low- and high-maginification TEM images and corresponding histograms of Pt particle size distributions of the GNS/Pt (a, b, and c) and PA-GNS/Pt (d, e, and f). The inset of d is a high-resolution transmission electron microscopy image of PA-GNS/Pt.

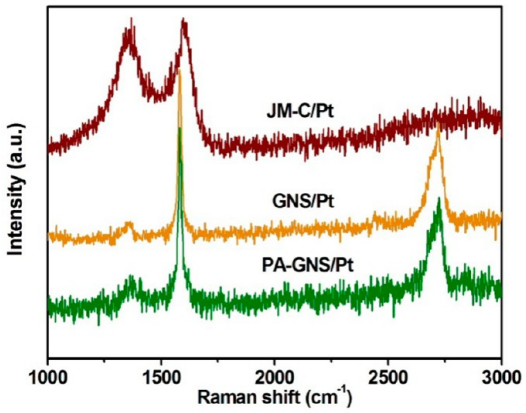

Figure 6. Raman spectra of JM-C/Pt, GNS/Pt, and PA-GNS/Pt.

electronic conductivity,[49] which plays a vital role in the electrocatalytic activity. And finally, in contrast to GNS/Pt electrode, the PA-GNS/Pt sample has sufficient amino groups, which helps improve the wettability and accessibility of methanol to the catalyst surface.[47]

The effect of PA on the stability of catalysts was investigated through accelerated durability test (ADT). Generally, it is believed that the loss of ECSA is the main reason for the degradation of the catalyst performance.[50] As shown in Figure 8, the ECSA of all catalysts decreases with the number of potential cycles under the ADT of DMFC conditions. After 500 cycles, PA-GNS/Pt retains 75.0% of the initial ECSA and 50.1% of the initial ECSA for GNS/Pt remained. However, only 21.5% of the initial ECSA for the JM-C/Pt remained after the same cycles. Among all the catalysts in this study, PA-GNS/Pt

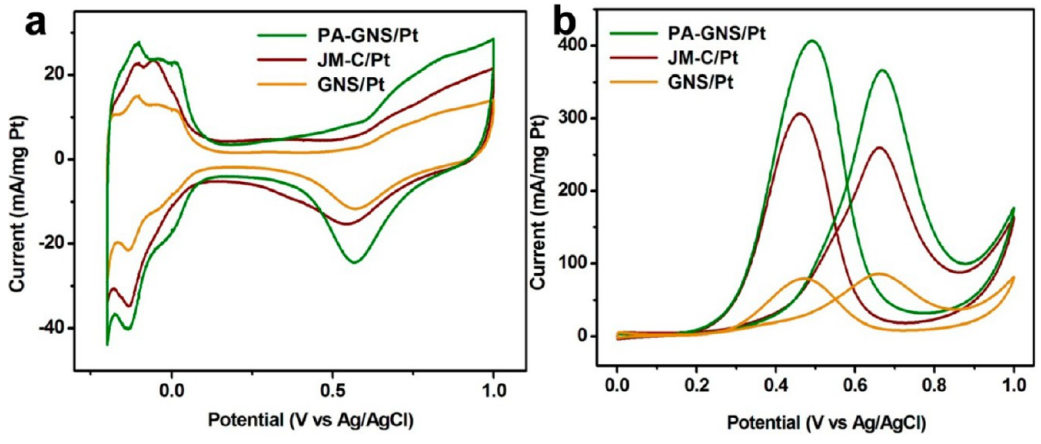

Figure 7. (a) CV for GNS/Pt, PA-GNS/Pt, and JM-C/Pt in 0.5 M H_2SO_4 solution at a scan rate of 25 mV s^{-1}. (b) CV for GNS/Pt, PA-GNS/Pt, and JM-C/Pt in 0.5 M H_2SO_4 + 1 M CH_3OH solution at a scan rate of 25 mV s^{-1}.

dx.doi.org/10.1021/sc4000016 | ACS Sustainable Chem. Eng. 2013, 1, 527−533

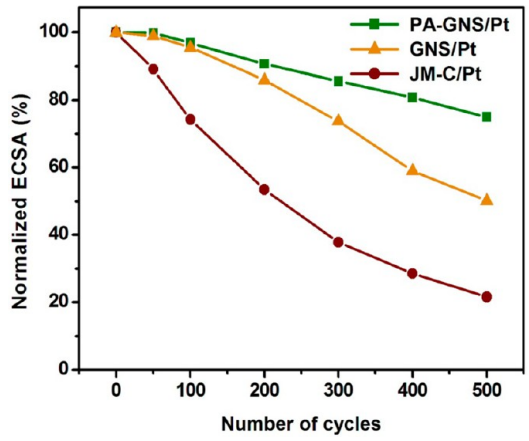

Figure 8. Normalized electrochemical active surface area based on cycle numbers during accelerated durability test.

shows the highest electrochemical stability, up to 3.5 times higher than that of JM-C/Pt and 1.5 times higher than that of GNS/Pt. The low stability of JM-C/Pt can be caused by the electrochemical carbon corrosion which makes the Pt particles detach from the support due to the low degree of graphitization.[50,51] As for GNS/Pt and PA-GNS/Pt, the improved stability of them is due to the low defect density and high degree of graphitization which impart them with excellent electrochemical corrosion resistance.[50] But for the GNS/Pt, the loss of ECSA might be caused by Pt conglomeration. Due to the fact that the surface of pristine graphene nanosheets is relatively inert, Pt nanoparticles are typically weakly adsorbed on graphene and easy to migrate along the surface which leads to Pt nanoparticles aggregating into larger particles.[30,44] By contrast, the greatly improved durability of the PA modified GNS can be ascribed to the strong interaction between PA and GNS,[41] because PA can serve as interlinkers and effective barriers to prevent the Pt nanoparticles from sintering.[39] In addition, the graphitic structure of PA-GNS can be retained even the outmost layer is corroded.[32]

CONCLUSIONS

In summary, we successfully prepared PA noncovalent modificated graphene nanosheets and their further functionalization with Pt nanoparticles. The obtained catalyst of Pt nanoparticles supported on PA-GNS exhibited higher electrochemical active surface area, better methanol catalytic activity, and long-term stability compared with the commercial catalyst JM-C/Pt and GNS/Pt. The enhanced performance of PA-GNS/Pt can be ascribed to the following: (1) the intact structure of graphene nanosheets due to the noncovalent modification, as well as the excellent electronic conductivity and resistance to corrosion, is maintained; (2) the introduction of PA offers a desirable active site for Pt nanoparticles anchoring and improves their dispersion on GNS with a smaller size and narrower size distribution, as well as introducing more active sites of Pt; (3) the remaining PA on the GNS can act as barriers to prevent the Pt nanoparticles from sintering and hence improve the stability of the catalyst. This indicates that PA-modified graphene nanosheets are a promising support material for DMFCs. Therefore, it is a positive strategy to exfoliate graphite to graphene using SC CO_2 and further functionalization with metal nanoparticles, and it is expected to help us to achieve wider application in environmental and energy fields.

AUTHOR INFORMATION

Corresponding Author

*E-mail: qunxu@zzu.edu.cn.

Notes

The authors declare no competing financial interest.

ACKNOWLEDGMENTS

We are grateful for the National Natural Science Foundation of China (No. 51173170, 21101141, 50955010, 20974102), Program for Excellent Scientist from Henan province (No. 114200510019), and the financial support from the Program for New Century Excellent Talents in University (NCET).

REFERENCES

(1) Winter, M.; Brodd, R. J. What are batteries, fuel cells, and supercapacitors? *Chem. Rev.* **2004**, *104*, 4245−4270.
(2) Lubitz, W.; Tumas, W. Hydrogen: An overview. *Chem. Rev.* **2007**, *107*, 3900−3903.
(3) Milliken, J.; Joseck, F.; Wang, M.; Yuzugullu, E. The advanced energy initiative. *J. Power Sources* **2007**, *172*, 121−131.
(4) Sundmacher, K. Fuel cell engineering: Toward the design of efficient electrochemical power plants. *Ind. Eng. Chem. Res.* **2010**, *49*, 10159−10182.
(5) Aricò, A. S.; Srinivasan, S.; Antonucci, V. DMFCs: From fundamental aspects to technology development. *Fuel Cells* **2001**, *1*, 133−161.
(6) Bianchini, C.; Shen, P. K. Palladium-based electrocatalysts for alcohol oxidation in half cells and in direct alcohol fuel cells. *Chem. Rev.* **2009**, *109*, 4183−4206.
(7) Qiao, Y.; Li, C. M. Nanostructured catalysts in fuel cells. *J. Mater. Chem.* **2011**, *21*, 4027−4036.
(8) Xu, J.; Fu, G.; Tang, Y.; Zhou, Y.; Chen, Y.; Lu, T. One-pot synthesis of three-dimensional platinum nanochain networks as stable and active electrocatalysts for oxygen reduction reactions. *J. Mater. Chem.* **2012**, *22*, 13585−13590.
(9) Rao, C. V.; Viswanathan, B. Monodispersed platinum nanoparticle supported carbon electrodes for hydrogen oxidation and oxygen reduction in proton exchange membrane fuel cells. *J. Phys. Chem. C* **2010**, *114*, 8661−8667.
(10) Zhao, X.; Yin, M.; Ma, L.; Liang, L.; Liu, C.; Liao, J.; Lu, T.; Xing, W. Recent advances in catalysts for direct methanol fuel cells. *Energy Environ. Sci.* **2011**, *4*, 2736−2753.
(11) Xu, Y.; Hou, S.; Liu, Y.; Zhang, Y.; Wang, H.; Zhang, B. Facile one-step room-temperature synthesis of Pt_3Ni nanoparticle networks with improved electro-catalytic properties. *Chem. Commun.* **2012**, *48*, 2665−2667.
(12) Mazumder, V.; Lee, Y.; Sun, S. Recent development of active nanoparticle catalysts for fuel cell reactions. *Adv. Funct. Mater.* **2010**, *20*, 1224−1231.
(13) Guo, S.; Wang, E. Noble metal nanomaterials: Controllable synthesis and application in fuel cells and analytical sensors. *Nano Today* **2011**, *6*, 240−264.
(14) Bing, Y.; Liu, H.; Zhang, L.; Ghosh, D.; Zhang, J. Nanostructured pt-alloy electrocatalysts for PEM fuel cell oxygen reduction reaction. *Chem. Soc. Rev.* **2010**, *39*, 2184−2202.
(15) Ravikumar, M. K.; Shukla, A. K. Effect of methanol crossover in a liquid-feed polymer-electrolyte direct methanol fuel cell. *J. Electrochem. Soc.* **1996**, *143*, 2601−2606.
(16) Auer, E.; Freund, A.; Pietsch, J.; Tacke, T. Carbons as supports for industrial precious metal catalysts. *Appl. Catal. A: Gen.* **1998**, *173*, 259−271.
(17) Li, W.; Liang, C.; Zhou, W.; Qiu, J.; Zhou; Sun, G.; Xin, Q. Preparation and characterization of multiwalled carbon nanotube-

supported platinum for cathode catalysts of direct methanol fuel cells. *J. Phys. Chem. B* **2003**, *107*, 6292−6299.
(18) Wang, C.; Waje, M.; Wang, X.; Tang, J. M.; Haddon, R. C.; Yan.. Proton exchange membrane fuel cells with carbon nanotube based electrodes. *Nano Lett.* **2003**, *4*, 345−348.
(19) Zhang, W.; Chen, J.; Swiegers, G. F.; Ma, Z.-F.; Wallace, G. G. Microwave-assisted synthesis of Pt/CNT nanocomposite electrocatalysts for PEM fuel cells. *Nanoscale* **2010**, *2*, 282−286.
(20) Chen, J.; Wang, M.; Liu, B.; Fan, Z.; Cui, K.; Kuang, Y. Platinum catalysts prepared with functional carbon nanotube defects and its improved catalytic performance for methanol oxidation. *J. Phys. Chem. B* **2006**, *110*, 11775−11779.
(21) Hsin, Y. L.; Hwang, K. C.; Yeh, C.-T. Poly(vinylpyrrolidone)-modified graphite carbon nanofibers as promising supports for PtRu catalysts in direct methanol fuel cells. *J. Am. Chem. Soc.* **2007**, *129*, 9999−10010.
(22) Oh, H.-S.; Kim, H.-S. Noncovalent modification of carbon nanofibers using 2-naphthalenethiol for catalyst supports in PEM fuel cells. *J. Electrochem. Soc. Tech.* **2010**, *1*, 92−96.
(23) Shang, N.; Papakonstantinou, P.; Wang, P.; Silva, S. R. P. Platinum integrated graphene for methanol fuel cells. *J. Phys. Chem. C* **2010**, *114*, 15837−15841.
(24) Kou, R.; Shao, Y.; Mei, D.; Nie, Z.; Wang, D.; Wang, C.; Viswanathan, V. V.; Park, S.; Aksay, I. A.; Lin, Y.; Wang, Y.; Liu, J. Stabilization of electrocatalytic metal nanoparticles at metal−metal oxide−graphene triple junction points. *J. Am. Chem. Soc.* **2011**, *133*, 2541−2547.
(25) Yoo, E.; Okata, T.; Akita, T.; Kohyama, M.; Nakamura, J.; Honma, I. Enhanced electrocatalytic activity of Pt subnanoclusters on graphene nanosheet surface. *Nano Lett.* **2009**, *9*, 2255−2259.
(26) Geim, A. K.; Novoselov, K. S. The rise of graphene. *Nat. Mater.* **2007**, *6*, 183−191.
(27) Huang, C.; Li, C.; Shi, G. Graphene based catalysts. *Energy Environ. Sci.* **2012**, *5*, 8848−8868.
(28) Huang, X.; Qi, X.; Boey, F.; Zhang, H. Graphene-based composites. *Chem. Soc. Rev.* **2012**, *41*, 666−686.
(29) Huang, X.; Yin, Z.; Wu, S.; Qi, X.; He, Q.; Zhang, Q.; Yan, Q.; Boey, F.; Zhang, H. Graphene-based materials: Synthesis, characterization, properties, and applications. *Small* **2011**, *7*, 1876−1902.
(30) Gan, Y.; Sun, L.; Banhart, F. One- and two-dimensional diffusion of metal atoms in graphene. *Small* **2008**, *4*, 587−591.
(31) Oh, H.-S.; Lim, K. H.; Roh, B.; Hwang, I.; Kim, H. Corrosion resistance and sintering effect of carbon supports in polymer electrolyte membrane fuel cells. *Electrochim. Acta* **2009**, *54*, 6515−6521.
(32) Huang, H.; Chen, H.; Sun, D.; Wang, X. Graphene nanoplate-Pt composite as a high performance electrocatalyst for direct methanol fuel cells. *J. Power Sources* **2012**, *204*, 46−52.
(33) Kundu, P.; Nethravathi, C.; Deshpande, P. A.; Rajamathi, M.; Madras, G.; Ravishankar, N. Ultrafast microwave-assisted route to surfactant-free ultrafine Pt nanoparticles on graphene: Synergistic co-reduction mechanism and high catalytic activity. *Chem. Mater.* **2011**, *23*, 2772−2780.
(34) Fampiou, I.; Ramasubramaniam, A. Binding of Pt nanoclusters to point defects in graphene: Adsorption, morphology, and electronic structure. *J. Phys. Chem. C* **2012**, *116*, 6543−6555.
(35) Vedala, H.; Sorescu, D. C.; Kotchey, G. P.; Star, A. Chemical sensitivity of graphene edges decorated with metal nanoparticles. *Nano Lett.* **2011**, *11*, 2342−2347.
(36) Barinov, A.; Malcioğlu, O. B.; Fabris, S.; Sun, T.; Gregoratti, L.; Dalmiglio, M.; Kiskinova, M. Initial stages of oxidation on graphitic surfaces: Photoemission study and density functional theory calculations. *J. Phys. Chem. C* **2009**, *113*, 9009−9013.
(37) Wang, S.; Wang, X.; Jiang, S. P. PtRu nanoparticles supported on 1-aminopyrene-functionalized multiwalled carbon nanotubes and their electrocatalytic activity for methanol oxidation. *Langmuir* **2008**, *24*, 10505−10512.
(38) Li, X. L.; Liu, Y. Q.; Fu, L.; Cao, L. C.; Wei, D. C.; Wang, Y. Efficient synthesis of carbon nanotube−nanoparticle hybrids. *Adv. Funct. Mater.* **2006**, *16*, 2431−2437.
(39) Oh, H.-S.; Kim, H. Efficient synthesis of Pt nanoparticles supported on hydrophobic graphitized carbon nanofibers for electrocatalysts using noncovalent functionalization. *Adv. Funct. Mater* **2011**, *21*, 3954−3960.
(40) Zheng, X.; Xu, Q.; Li, J.; Li, L.; Wei, J. High-throughput, direct exfoliation of graphite to graphene via a cooperation of supercritical CO_2 and pyrene-polymers. *RSC Adv.* **2012**, *2*, 10632−10638.
(41) Li, L.; Zheng, X.; Wang, J.; Sun, Q.; Xu, Q. Solvent-exfoliated and functionalized graphene with assistance of supercritical carbon dioxide. *ACS Sustainable Chem. Eng.* **2013**, *1*, 144−151.
(42) Zoval, J. V.; Lee, J.; Gorer, S.; Penner, R. M. Electrochemical preparation of platinum nanocrystallites with size selectivity on basal plane oriented graphite surfaces. *J. Phys. Chem. B* **1998**, *102*, 1166−1175.
(43) Radmilovic, V.; Gasteiger, H. A.; Ross, P. N. Structure and chemical composition of a supported Pt-Ru electrocatalyst for methanol oxidation. *J. Catal.* **1995**, *154*, 98−106.
(44) Morrow, B. H.; Striolo, A. Platinum nanoparticles on carbonaceous materials: The effect of support geometry on nanoparticle mobility, morphology, and melting. *Nanotechnology* **2008**, *19*, 195711.
(45) Knights, S. D.; Colbow, K. M.; St-Pierre, J.; Wilkinson, D. P. Aging mechanisms and lifetime of PEFC and DMFC. *J. Power Sources* **2004**, *127*, 127−134.
(46) Strano, M. S.; Dyke, C. A.; Usrey, M. L.; Barone, P. W.; Allen, M. J.; Shan, H.; Kittrell, C.; Hauge, R. H.; Tour, J. M.; Smalley, R. E. Electronic structure control of single-walled carbon nanotube functionalization. *Science* **2003**, *301*, 1519−1522.
(47) Sharma, S.; Ganguly, A.; Papakonstantinou, P.; Miao, X.; Li, M.; Hutchison, J. L.; Delichatsios, M.; Ukleja, S. Rapid microwave synthesis of CO tolerant reduced graphene oxide-supported platinum electrocatalysts for oxidation of methanol. *J. Phys. Chem. C* **2010**, *114*, 19459−19466.
(48) Khosravi, M.; Amini, M. K. Flame synthesis of carbon nanofibers on carbon paper: Physicochemical characterization and application as catalyst support for methanol oxidation. *Carbon* **2010**, *48*, 3131−3138.
(49) Xin, Y.; Liu, J.-g.; Jie, X.; Liu, W.; Liu, F.; Yin, Y.; Gu, J.; Zou, Z. Preparation and electrochemical characterization of nitrogen doped graphene by microwave as supporting materials for fuel cell catalysts. *Electrochim. Acta* **2012**, *60*, 354−358.
(50) Wang, J.; Yin, G.; Shao, Y.; Wang, Z.; Gao, Y. Investigation of further improvement of platinum catalyst durability with highly graphitized carbon nanotubes support. *J. Phys. Chem. C* **2008**, *112*, 5784−5789.
(51) Kangasniemi, K. H.; Condit, D. A.; Jarvi, T. D. Characterization of vulcan electrochemically oxidized under simulated PEM fuel cell conditions. *J. Electrochem. Soc.* **2004**, *151*, E125−E132.